A measurement-based distributed large-signal E/O circuit model for high-speed electroabsorption modulators

F. Cappelluti, M. Pirola and G. Ghione
Dipartimento di Elettronica and CERCOM, Politecnico di Torino,
corso Duca degli Abruzzi 24, I-10129 Torino, Italy.
Phone +39 11 564 4165, Fax +39 11 564 4099, E-mail: federica.cappelluti@polito.it

***Abstract*— The paper presents a measurement-based large-signal distributed model for high-speed electroabsorption modulators, integrated within an RF circuit CAD environment. The model is implemented through a cascaded-cell approach; the identification of the nonlinear lumped equivalent circuit parameters of each cell through measurements is discussed and an example is provided of circuit extraction. An example of integrated driver-EAM simulation is finally discussed.**

I. Introduction

Electroabsorption modulators (EAMs) offer great potential for the development of low-cost integrated transmitters and combined receiver/transmitter units in high-speed digital and/or analog fiber-optic transmission systems. Often the EAM can be directly integrated with the laser; the corresponding device is usually referred to as EAL. Although in the rest of the paper reference is made to EAMs, the approach also applies to the modulating section of an EAL provided that the source and modulator are decoupled (i.e. the source is optically isolated from the EAM).

EAMs usually make use of a *p-i-n* structure, in which the optical absorption and the related refractive index are modulated by varying the electric field across the intrinsic layer. They can be designed either as lumped or travelling-wave (TW-EAM) devices, the latter offering better performance in terms of bandwidth, efficiency and saturation optical power [1]. In the lumped configuration the microwave signal is usually applied to the center of the electrode (see Fig. 1, right), while in the TW design (see Fig. 1, left) the microwave signal is made co-propagate with the optical signal, and the waveguide is terminated by a matched load. Due to the high microwave and optical losses, the device length is limited to a few hundreds micrometers even in the TW design; however, a significant transmission line-like behavior and response broadbanding is observed provided that the load is impedance matched to the electrode characteristic impedance; since this is usually significantly lower than 50 Ω, careful design of the termination load and of the driver electronics is required. Thus, despite the electrically short length, the use of a distributed approach is generally more effective, not least owing to the space-dependent optical power distribution along the line [2].

A self-consistent EAM electrical and optical model within a microwave circuit CAD environment is important both for the modulator RF design and for the co-design and optimization of integrated modulator-driver circuits [3], which requires to accurately model these not only from the RF but also from the optical standpoint (amplitude modulation and chirp); this

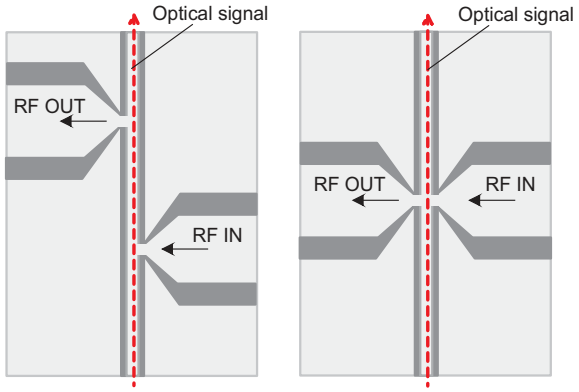

Fig. 1. EAM layouts: travelling-wave electrode (left), lumped electrode (right).

ultimately allows to simulate the driver-modulator pair at a system level, possibly with a direct link to the RF circuit CAD environment, as today possible within many commercially available CAD suites.

Following a cascaded-cell approach, well suited thanks to the electrically short length of such devices (in contrast with $LiNbO_3$-based electro-optic modulators), a self-consistent, nonlinear electro-optic EAM model yielding not only the RF electrical behaviour and the output optical power amplitude modulation, but also its spurious phase modulation (chirp) has been recently proposed by the present authors [4]. The current implementation is within the MWOFFICE design suite [5], but the model can be readily exported to other RF design environments. The model structure allows for frequency-domain small-signal and large-signal (through Harmonic Balance techniques) analysis.

The CAD model was originally developed as physics-based, i.e. the EAM line parameters were derived from a self-consistent electromagnetic and semiconductor model [6] and the voltage dependence of the absorption and effective index deviation was taken from a microscopic model, together with the RF-optical overlap integral. However, the same framework can be exploited, as discussed in the present paper, to derive a measurement-based model. In fact, we show that the (linear and nonlinear) circuit element models, i.e. their dependence on the local voltage and optical power, can be reliably identified on the basis of external (electrical and eletro-optical) measurements. As a validation example, we start from a full distributed physics-based model of an InP/InGaAsP EAM,

either in TW or lumped configuration, and identify the circuit model on the basis of simulated external measurements. This allows to include all the physical relevant issues but avoiding uncertainties inherently related to real measured data, e.g. due to parasitic deembedding.

II. Circuit Model

Following the approach outlined in [2], the modulator model is made of coupled transmission lines (TL), modelling the microwave and the optical waveguide, respectively. Coupling is obtained through the inclusion of a voltage and optical power dependent photocurrent generator in the microwave TL, while, in turn, the microwave voltage drives the absorption and refractive index deviation in the optical waveguide. Within the CAD circuit environment, the nonuniform, nonlinear microwave and optical waveguides are simulated through a cascaded-cell approach, employing both standard and user-defined lumped elements. Excellent accuracy may be achieved provided that the unit-cell length is short enough with respect either to the absorption length or the microwave guided wavelength in the frequency range of interest [4].

The schematic of a unit-cell equivalent circuit is shown in Fig. 2. The circuit between the electrical ports 1 and 2 models a Δz-long section of the nonlinear microwave electrode, treated as equivalent to a quasi-TEM transmission line, whose propagation characteristics are modeled by the conduction resistance $R_{\rm con}(f)$, the (unloaded) TL inductance and capacitance (L, C), the *p-i-n* junction series resistance ($R_{\rm S}$), the voltage-dependent capacitance ($C_{\rm j}(V_{\rm j})$), and the optical-controlled photocurrent generator $I_{\rm ph}$. The circuit between the optical ports 3 and 4 models the optical intensity (associated to an equivalent voltage) modulation and drives the photocurrent generator through:

$$I_{\rm ph} = \frac{q}{\hbar\omega_{\rm o}} P_{\rm in}\left(1 - T_{\Delta z}\left(V_{\rm j}, P_{\rm in}\right)\right) \tag{1}$$

$$T_{\Delta z}\left(V_{\rm j}, P_{\rm in}\right) = {\rm e}^{-\Gamma_{\rm o}\alpha\left(V_{\rm j}, P_{\rm in}\right)\Delta z} \tag{2}$$

$$\alpha\left(V_{\rm j}, P_{\rm in}\right) = \frac{\alpha_{\rm m}\left(V_{\rm j}\right)}{1 + P_{\rm in}/P_{\rm th}\left(V_{\rm j}\right)} \tag{3}$$

where q is the electric charge, $\hbar$ is the Planck constant, $\omega_{\rm o}$ is the optical angular frequency, and $P_{\rm in}$ is the optical power incident on the section. $T_{\Delta z}\left(V_{\rm j}, P_{\rm in}\right)$ is the Δz-section transmission which is computed through a user-defined block model implementing equations (2-3). In (2-3) Γ_o is the optical confinement factor in the active layer, $\alpha_{\rm m}$ is the active material optical absorption, while the term $1/(1+P_{\rm in}/P_{\rm th})$ is a heuristic corrective factor introduced to account for saturation effects arising at high optical power levels. Finally a time delay block describes the optical envelope propagation and allows to simply include velocity-mismatch effect. The last circuit, connecting the optical ports 5 and 6, models the spurious optical phase modulation (associated to an equivalent voltage) induced by the electric-field modulated optical refractive index ($\Delta n_{\rm m}$), according to eq. (4). Finally, a simple derivation block at the end of the multi-section circuit is used to directly evaluate the instantaneous frequency chirp.

$$\phi_{\rm out} = \phi_{\rm in} + \Delta\phi(V_{\rm j}, P_{\rm inj}) = \phi_{\rm in} - \frac{\omega_{\rm o}}{c}\Delta n_{\rm m}\left(V_{\rm j}, P_{\rm op}\right)\Delta z. \tag{4}$$

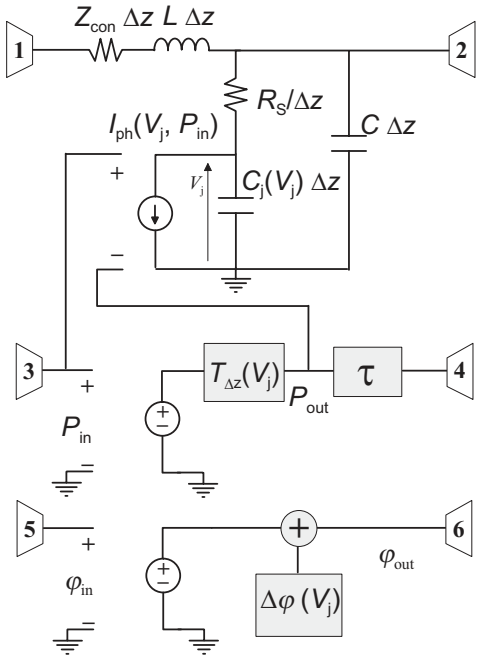

Fig. 2. Circuit schematic of a Δz-long modulator unit cell.

III. Circuit Parameter Extraction

The proposed model indeed requires the knowledge of microwave and optical waveguide parameters; these can be accurately extracted from standard eletro-optic and electrical characterization tools.

Concerning the model optical parameters, the effective optical absorption $\Gamma_{\rm o}\alpha(V)$ and the saturation parameter $P_{\rm th}$ can be accurately extracted through low-frequency measurements of the modulator transmission and photocurrent (see e.g. [7], [8]), while the chirp parameter, and thus of $\Delta n_{\rm m}(V)$, can be derived from small-signal measurements at different bias conditions, as outlined in [9].

The identification of the electrical circuit elements can be performed from the measured two-port electrical S-parameters or, for packaged devices internally terminated, from the measured electric return loss (S_{11}).

In order to provide a reliable validation to the extraction procedure, this has been tested by performing simulated measurements on the accurate physics-based cascaded-cell model in [4]. We consider a bulk InP/InGaAsP EAM whose cross-section and simulated characteristic impedance are reported in Fig. 3; further details on the device may be found in [4]. Two different layouts, exploiting a TW electrode and a lumped electrode of equal length (500 μm) and cross-section, have been analyzed.

Fig. 5 shows the simulated S_{11} for the TW and lumped EAM. Both the modulators were closed on a 23 Ω load. While the TWEAM S_{11} remains limited even at high frequency, thus confirming the transmission line like behavior, the lumped EAM presents return loss increasing with frequency, as expected for an *RC* limited device. In view of this result, we have fitted the lumped S_{11} with an equivalent, electrically lumped circuit, as shown in Fig. 4. The agreement between the original and the fitted circuit in terms of S_{11} is excellent up to 40 GHz, where the guided wavelength becomes comparable to the electrode length, so that the distributed feature of the electrode

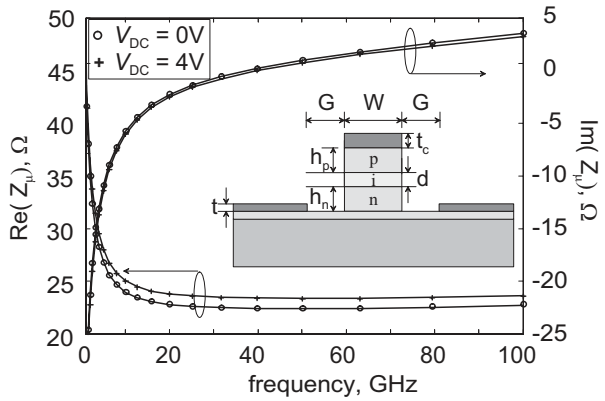

Fig. 3. EAM characteristic impedance computed from [6] (line) and from the cascaded-cell equivalent circuit (symbols).

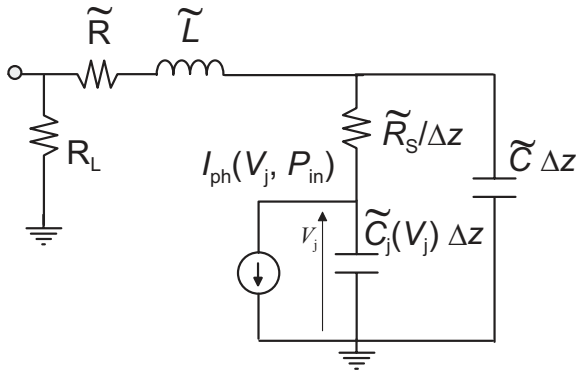

Fig. 4. Circuit schematic of the single-cell extracted circuit for the lumped electrode configuration. Only the electrical part is shown; connection to the optical waveguide is the same as in Fig. 2.

cannot be longer neglected. As far as the TW electrode, by knowing the modulator length, the series resistance and inductance ($R_{\rm con}$ and L) can be extracted from the low- and high-frequency values of S_{11}. Then, the parallel branch components are obtained by fitting the S_{11} frequency behavior; S_{11} measurements at different working point may allow for the voltage dependence extraction of the junction capacitance.

Fig. 6 (top) shows the calculated electro-optic response for the original TW and lumped modulators, and for the modulator simulated by exploiting the extracted fitted circuit in Fig. 4. The incident optical power and input RF signal are 0 dBm and 1 mV, respectively. The electro-optic response frequency behavior reflects the features of S_{11}, showing the significant advantage of the TW configuration compared to the lumped one, for a given device capacitance. A good agreement between the original lumped EAM and its extracted equivalent model is observed within the -3 dB bandwidth, while a significant inaccuracy arises at high frequencies, due to the approximation of the electrode with a lumped circuit. The comparison is even worse at higher optical power (see Fig. 6 , bottom) owing to the distributed nonuniform feature of the optical waveguide, not taken into account in the single-cell equivalent circuit model. These results point out that the extraction of an accurate broadband model of the EAM requires a detailed knowledge of the device structure. On the other hand, in the low-frequency range, as suggested also from the circuit topology, the single-cell approach accurately captures the small-signal response, thus confirming the correctness

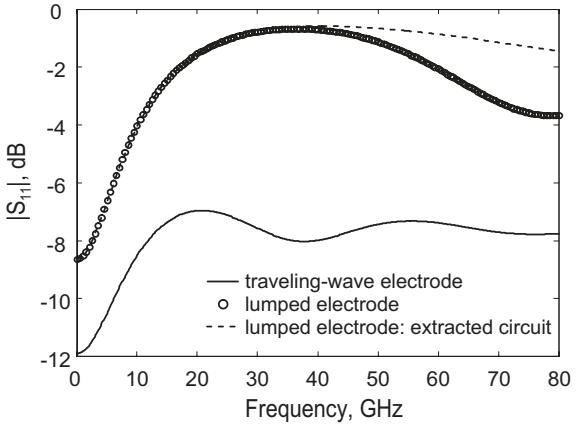

Fig. 5. Comparison of the electrical return loss of the devices with travelling wave and lumped layout. For the lumped case, also the return loss computed from the extracted single-cell equivalent circuit in Fig. 4 is reported.

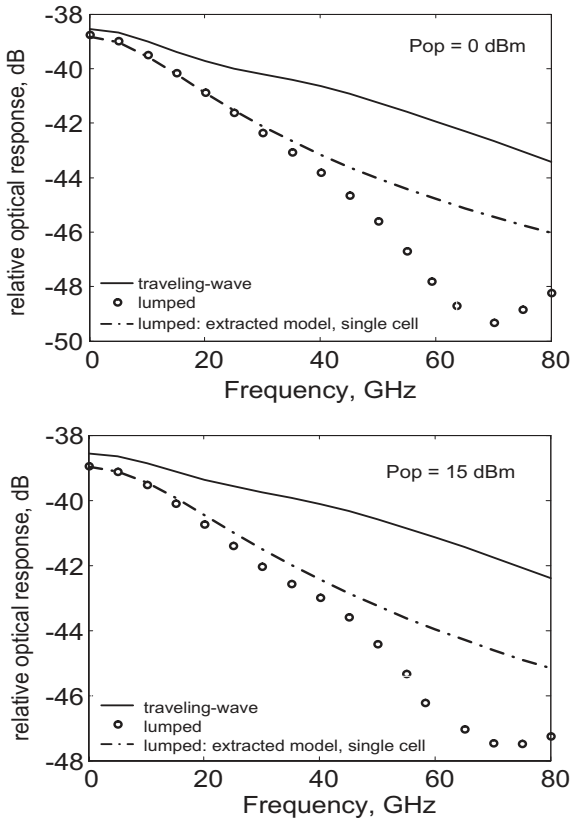

Fig. 6. Small signal optical response, at 0 dBm (top) and 15 dBm (bottom) incident optical power. The response is normalized to the input optical power.

of using low-frequency optical transmission measurements to identify the effective optical absorption.

IV. Driver / EAM simulation

As an example of application of the circuit CAD modelling approach, in this section we investigate the influence of the driver-EAM design on the transmission performance of a 10-Gb/s EAL module. EALs are key devices for the development of low cost optical transmission systems in the Metro Network segments over dispersive fiber, and many studies are currently carried out on the development of new transmission techniques, exploiting e.g. electronic pulse shaping, in order to reduce or even remove the need for dispersion compensation on the optical link. In this framework a key aspect is the

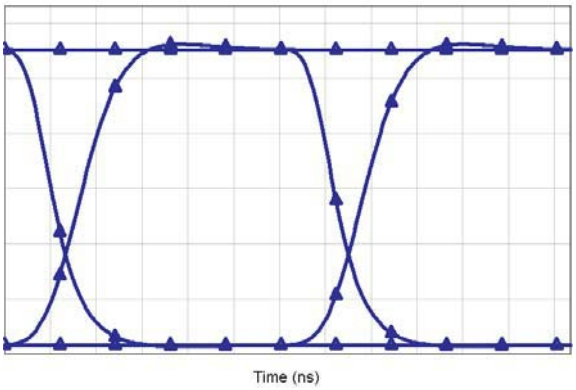

Fig. 7. Simulated optical eye diagram of the EAM under 10 Gb/s NRZ modulation.

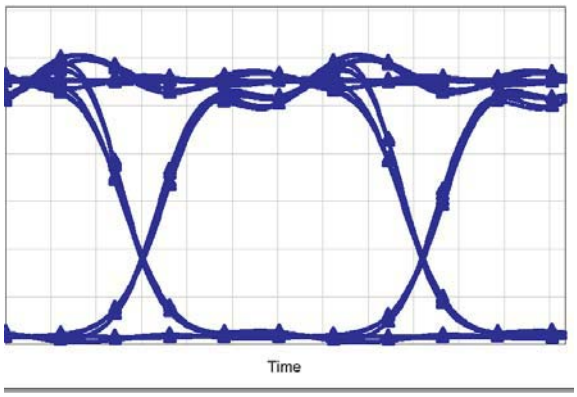

Fig. 8. Simulated optical eye diagram of the driver-EAM pair under 10 Gb/s NRZ modulation.

capability to predict how the optical transmission performance are affected not only from the modulator but from the driver-EAM pair.

Concerning the EAM, the analysis has been carrier out by exploiting a large-signal lumped model extracted from small-signal electro-optic measurements under different incident optical power [10]. The EAM is loaded on a 50 Ω load. In order to assess the modulator capability for 10-Gb/s NRZ transmission, a 256-long PRBS square-wave shaped signal is applied, with 0.9 V peak-to-peak and -0.2 V offset for mark bits. The RF generator impedance is 50 Ω. The maximum output optical power is 1 dBm with an extinction ratio of about 9 dB. The resulting eye-diagram after 0 km of fiber is shown in Fig. 7. A small overshoot of the optical signal is observed on the mark due to impedance mismatch at high frequencies. Then, the modulator has been coupled to the driver, whose frequency response is approximated by a fourth-order Bessel Filter with -3dB frequency cutoff of 10 GHz. The driver low frequency impedance is 50 Ω. The simulated eye-diagram is reported in Fig. 8, showing significantly increased overshoot at the mark and undershoot at the space due to the increased impedance mismatch induced by the driver. The measured eye-diagram is reported in Fig. 9. The optical pulse shape may affect in a significant way the EAL transmission performance [11]; moreover, due to the nonlinear feature of the EAM transfer curve, the overshoot amplitude increases at higher reverse applied voltage, which is desirable to obtain negative chirp. Thus, driving signal optimization demands for accurate modelling of frequency chirp as well as of pulse shape.

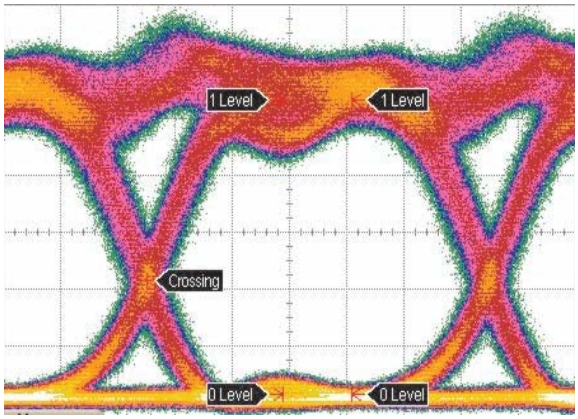

Fig. 9. Measured optical eye diagram at 10 Gb/s under NRZ modulation.

V. Conclusion

The paper has presented a measurement-based large-signal distributed model for high-speed EAMs integrated within an RF circuit CAD environment. The identification of the non-linear equivalent circuit parameters through measurements has been discussed together with an example of circuit extraction. Finally, an example of integrated driver-EAM simulation has been presented.

Acknowledgement

This work has been partly supported by CISCO under the University Research Program "Investigation of the use of very low-cost lasers in the 10 GigE WDM Metro Environment".

References

[1] S. Irmscher, R. Lewen, and U. Eriksson, "InP/InGaAsP high-speed travelling-wave electro-absorption modulators with integrated termination resistors", *IEEE Photon. Technol. Lett.*, Vol. 14, No.7, pp. 923-925, July 2002.

[2] F. Cappelluti, G. Ghione: "Self-Consistent Time-Domain Large-Signal Model of High-Speed travelling-Wave Electroabsorption Modulators", *IEEE Trans. Microwave Theory Tech* , Vol. 51, No. 4, pp. 1196-1104, April 2003.

[3] M. Pirola, F. Cappelluti, G. Giarola, G. Ghione, "Multi-Sectional modelling of High-Speed Electro-Optic Modulators Integrated in a Microwave Circuit CAD Environment", to be published in *IEEE J. Lightwave Technol.*

[4] F. Cappelluti, A. Mela, M. Pirola, G. Ghione, "Large-signal E/O modelling of travelling-wave electroabsorption modulators in an RF circuit CAD environment", *IEEE MTT-S Int. Microwave Symp. Dig.*, pp. 769-772, June 2004.

[5] Microwave Office 2002 RF Design Suite ver. 5.53, Applied Wave Research Inc.

[6] F. Bertazzi, F. Cappelluti, F. Bonani, M. Goano, G. Ghione, "A novel coupled physics-based electromagnetic model of semiconductor travelling-wave structures for RF and optoelectronic applications", *GAAS 2003 Proceedings*, pp. 239-242, October 2003.

[7] M. K. Chin, "A simple method using photocurrent and power transmission for measuring the absorption coefficient in electroabsoprtion modulators", *IEEE Photon. Technol. Lett.*, Vol. 4, No.8, pp. 866-869, August 1992.

[8] B. Liu, J. Shim, Y. Chiu, A. Keating, J. Piprek, J.E. Bowers, "Analog characterization of low-voltage MQW travelling-wave electroabsorption modulators", *IEEE J. Lightwave Technol.*, Vol. 21, No. 12, pp. 3011–3019, Dec. 2003.

[9] F. Devaux, "Simple measurement of fiber dispersion and of chirp parameter of intensity modulated light emitter", *IEEE J. Lightwave Technol.*, Vol. 11, No. 12, pp. 1937–1940, Dec. 1993.

[10] E. Griseri, Private Report, April 2004.

[11] Y. Kim, S. Nam, S. Park, S. Lee, D. Jang, H.S. Kang, J. Jeong, "Novel and simple model of 10-Gb/s electroabsoprtion modulated lasers and its experimental validation of transmission performance due to overshoot of optical signals", *IEEE Photon. Technol. Lett.*, Vol. 15, No. 5, pp. 643-645, 2003.